APL Materials

Enhanced electro-mechanical coupling of TiN/$Ce_{0.8}Gd_{0.2}O_{1.9}$ thin film electrostrictor

Cite as: APL Mater. **7**, 071104 (2019); https://doi.org/10.1063/1.5091735
Submitted: 05 February 2019 . Accepted: 23 June 2019 . Published Online: 10 July 2019

Simone Santucci, Haiwu Zhang, Simone Sanna, Nini Pryds, and Vincenzo Esposito

Enhanced electro-mechanical coupling of TiN/$Ce_{0.8}Gd_{0.2}O_{1.9}$ thin film electrostrictor

Cite as: APL Mater. 7, 071104 (2019); doi: 10.1063/1.5091735
Submitted: 5 February 2019 • Accepted: 23 June 2019 •
Published Online: 10 July 2019

Simone Santucci,[a] Haiwu Zhang, Simone Sanna, Nini Pryds, and Vincenzo Esposito[a]

AFFILIATIONS

Department of Energy Conversion and Storage, Technical University of Denmark, Frederiksborgvej 399 Roskilde, Denmark

[a]Authors to whom correspondence should be addressed: sisan@dtu.dk and vies@dtu.dk

ABSTRACT

Gadolium doped ceria, Gd:CeO_2 (CGO), have recently been shown to possess an exceptional high electrostriction coefficient (Q), which is at the least three orders of magnitude larger than the best performing lead-based electrostrictors, e.g. $Pb(Mn_{1/3}Nb_{2/3})O_3$. Herein, we show that CGO thin films fabricated by a pulsed laser deposition method can be directly integrated onto the Si substrate by using TiN films of few nanometers as functional electrodes. The exceptional good coupling between TiN and $Ce_{0.8}Gd_{0.2}O_{1.9}$ yields a high electrostriction coefficient of $Q_e = 40\ m^4\ C^{-2}$ and a superior electrochemomechanical stability with respect to the metal electrodes.

Electrostrictive materials respond with mechanical strain when subjected to external electric fields. They are deployed as actuators or transducers in a wide field of applications, including electronics, robotics, and ultrasound imaging.[1–3]

Nowadays, the widely used electrostrictor materials are piezoelectric materials such as $Pb(Mn_{1/3}Nb_{2/3})O_3$ (PMN) which are toxic and are being banned to be used due to environmental concerns. This limits their future applications in new highly relevant fields such as electronic, medical, and biocompatible applications. Meanwhile, Pb is highly diffusive and is prone to react with the silicon.[4,5] Pb-based piezoelectrics are thus difficult to be integrated with silicon technology, e.g., for MEMS, NMES, and CMOS technology.[5,6] To overcome such issues, complex architectures with chemical barrier layers and crystallization seed layers at the support have been fabricated to avoid chemical interaction between the Si and the film.[7,8]

On an alternative path, recent studies disclosed an exceptional high electrostriction response in Pb-free defective metal oxides, in particular, in Gd-doped Ceria (CGO).[9–13] CGO not only is environmental friendly[14] but also it showed gigantic electrostriction with Q_e values above 17 $m^4\ C^{-2}$, or field electrostrictive coefficient of $M_e \approx 10^{-18}\ m^2/V^2$[15] that does not depends on the polarization of the sample [both values are usually reported; see Eq. (4) for conversion]. These values are higher or at least comparable with the best State-of-the-Art materials such as PMN ($Q = 0.002\ m^4\ C^{-2}$ and $M_e = 2 \times 10^{-18}\ m^2/V^2$),[16] $BaBi_2Nb_2O_9$ ($Q = 0.038\ m^4\ C^{-2}$ and $M_e = 4.9 \times 10^{-19}\ m^2/V^2$),[17] or $Na_{0.5}Bi_{0.5}TiO_3$ ($Q = 0.022\ m^4\ C^{-2}$ and $M_e = 1.51 \times 10^{-19}\ m^2/V^2$).[18,19] Unlike such classic electrostrictors, CGO based materials do not follow Newnham's law[20,21] that relates both dielectric and mechanical properties with the electrostriction coefficient.

Therefore, a different electromechanical mechanism is in play for oxygen defective metal oxides as compared with the standard electrostriction. $CeO_{2-\delta}$ has a centrosymmetric fluorite structure, where a central cerium cation is surrounded by eight oxygen anions and oxygen vacancies. Acceptor dopants, such as Gd^{3+}, promote the formation of oxygen vacancies ($V_O^{\cdot\cdot}$) in the lattice, e.g., 20 mol. % Gd doping ($Ce_{0.8}Gd_{0.2}O_{2-\delta}$) corresponds to 5 mol. % oxygen vacancies ($\delta = 0.1$).[9,12,22] According to Lubomirsky *et al.*,[9,12,23] oxygen vacancies trigger the giant electrostrictions by reducing the Ce–O bond length of the local Ce-coordination shell and increasing the Ce-$V_O^{\cdot\cdot}$ pair distance.[11] Under these conditions, electromechanically active $V_O^{\cdot\cdot}$-cation complexes are formed in the lattice and these induce a significant local distortion under the application of moderate electrical fields. In a thin film cantilever configuration, these properties are manifested by the generation of an exceptional in-plane high stress, up to 500 MPa, between the CGO thin film and the substrate.[9] This process is thought to be rather slow, as its magnitude decrease readily with the frequency.[10,11]

Evidence of such electromechanical performances has been confirmed recently by Hadad *et al.*,[24] by depositing CGO thin films on Si with different metal electrodes (Si/x/CGO/x, x = Al, Pt, Cr). They found that the electromechanical performances and stability of the CGO thin films depend critically on the electrodes used, making a rigorous characterization of the film itself difficult. CGO electrostrictive thin films deposited on metal electrodes often show mechanical decoupling during operation due to poor adhesion at the ceramic-metallic interface.[11,24–26]

Furthermore, cerium oxide is a refractory material, and conversely to Pb-based materials that need chemical barrier layers, it does not react with Si/SiO_2 substrates and is compatible with many materials for both low and high temperature uses.[27–29]

In this study, in order to overcome these limitations, we included $Ce_{0.8}Gd_{0.2}O_{1.9}$ thin films with titanium nitride (TiN) electrodes (TiN/CGO/TiN configuration) by Pulsed Laser Deposition (PLD). TiN has a rock-salt (NaCl) structure and shows excellent mechanical and electrical properties, such as low resistance ($\sigma \approx$ 200 S/cm at room temperature) and high chemical stability.[30,31] Therefore, TiN is an ideal candidate for Si integrated technologies and microelectronics such as electrodes, diffusion barriers, gates, or Schottky barrier contacts.[32–35] Coupling CGO with TiN can significantly simplify the integration procedures of these electrostrictors with Si-based technologies and microelectronics. Moreover, as a ceramic material, TiN is expected to provide superior crystallographic transport matches to CGO and chemical stability. As for a comparison, CGO thin films with a Au/CGO/TiN configuration were also fabricated to analyze stability and degradation behavior.

The $Ce_{0.8}Gd_{0.2}O_{1.9}$ target for the deposition was fabricated by synthetized $Ce_{0.8}Gd_{0.2}O_{1.9}$ powder following by uniaxial cold-pressing at 140 MPa and then sintered at 1723 K for 10 h. A high pure fluorite phase was observed for the as prepared targets.

CGO films with thicknesses of 800 and 1400 nm were deposited by PLD on a commercial [90 nm TiN/525 μm Si] substrate (*Prime Wafers*). The wavelength of the excimer laser is 248 nm, with a 20 Hz repetition rate, an output energy of 200 mJ, and a fluence of 3 J cm^{-2} (growth rate of 0.05 Å/pulse).[28] The deposition temperature was set to be 400 °C, and the target-substrate distance was fixed at ~72 mm. In order to avoid possible oxidation of TiN, the first 15 min of deposition was carried out with nitrogen flow at 10^{-3} mbar, after which it was switched to oxygen at 10^{-3} mbar. Then, for films with the TiN/CGO/TiN configuration, TiN was grown by PLD with a temperature of 600 °C and N_2 flow at 10^{-3} mbar. For films with the Au/CGO/TiN configuration, the Au top electrode was sputtered at room temperature with a Bal-Tec SCD 005 Sputter Coater. The samples were cut in beam shape: 7–8 mm wide and 15 mm long.

XRD analyses were performed with a Bruker D8 on deposited films. No secondary phases in the as deposited thin films were observed within the resolution limit of the instrument. Microstructure investigation and thickness measurement were carried out with the Zeiss Gemini-Merlin FE-SEM on the cross section of the samples.

For electromechanical characterization, one end of the beam sized samples was clamped and the other end was free to move [see Fig. 1(c)]. Vertical displacement at the free end was measured with a nanovibration analyzer with a single-beam laser interferometer (SIOS NA Analyzer). A sinusoidal electric field was applied with an Aim-TTI TGP 3100 function generator at frequency f = 100 mHz, and the contacts were made with tungsten tips. Based on the vertical displacements of the free end, the change in stress was calculated, and subsequently, the electrostriction coefficient was obtained. As the measured displacement d is much smaller than the beam length L (i.e., $d \ll L$), the change in curvature Δk is

$$\Delta k = \frac{2d}{L^2}. \tag{1}$$

Using this value, the in plane stress $\Delta\sigma$ was calculated using the Stoney formula

$$\Delta\sigma = \frac{Y_s}{1-\nu_s}\frac{t_s^2}{6t_f}\Delta k, \tag{2}$$

where Y_s and ν_s are Young's modulus and the Poisson ratio of the substrate and are 130 GPa and 0.28, respectively, for Si.[36] t_s and t_f are the thickness of the substrate and film, respectively. The field electrostriction coefficient M_e is then obtained with the equation

$$\Delta\sigma = Y_f * M_e * E^2, \tag{3}$$

where E is the external electric field applied and Y_s is Young's modulus of CGO (≈200 GPa).[9] In order to isolate harmonics

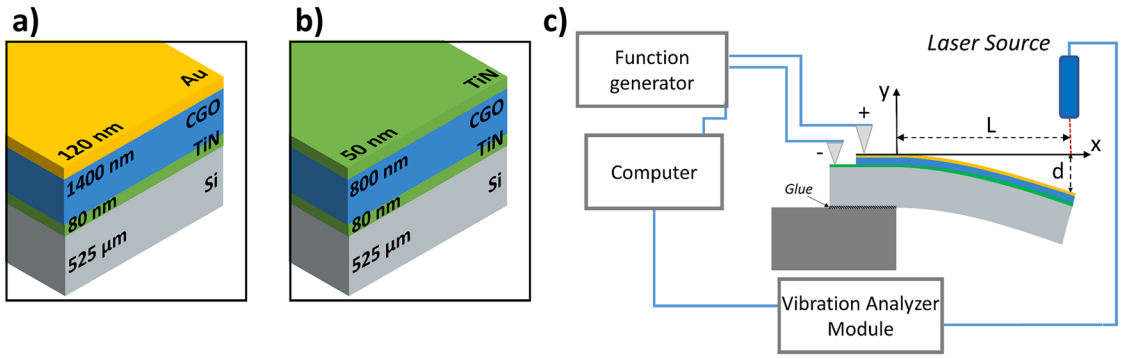

FIG. 1. Schematic illustration of the CGO thin films with (a) Au/CGO/TiN and (b) TiN/CGO/TiN configurations. (c) Schematic of the setup for beam deflection measurement. The dimension of the beam shaped samples is 7–8 mm * 15 mm.

oscillation, the signal was smoothed and the mechanical drift of the interferometer removed with a linear fit of the background.

Although the polarization electrostriction coefficient (Q_e) is generally used to describe the classic electrostrictors, the field electrostriction coefficient (M_e) is preferably used in the experimental procedure, as it is related to the electric field instead of polarization. M_e and Q_e coefficients are related by the equation

$$M_e = Q_e\{\varepsilon_0(\varepsilon_r - 1)\}^2, \quad (4)$$

where ε_0 is the vacuum permittivity and ε_r is the relative dielectric constant of CGO (≈28).[9,12,37,38] During the experiment, we tracked potential temperature variation with a FLIR SC5000 thermal camera with a waveband of 2.5–5.1 μm and 20 mK sensitivity.

The film quality is generally improved by increasing the temperature at the substrate (T_s) above 400 °C and by reducing the oxygen partial pressure (pO_2) within the PLD deposition chamber.[28,39,40] The substrate temperature (T_s) during PLD is a particularly important parameter to achieve high density of the CGO thin films, ensuring mechanical continuity of the electrostrictive film.[41] High crystallographic order is achieved, as CGO is deposited on structurally similar substrates with similar lattice parameters.[41,42] On the other hand, Infortuna *et al.*[39] found that $pO_2 < 5 \times 10^{-2}$ mbar promotes a dense columnar structure in CGO, above which disordered and porous microstructures were observed. The top TiN electrode was deposited at 600 °C to increase conductivity,[43] avoiding residual strain.[44] During the deposition, N_2 flow was used to avoid oxygen inclusion[43] and the variation of the stoichiometry of TiN. The correct stoichiometry was confirmed by XRD (Fig. S1 of the supplementary material).

Figures 1(a) and 1(b) schematically illustrate the configurations of Au/CGO/TiN and TiN/CGO/TiN, respectively. Structural and microstructural analyses reveal that the thickness of the bottom TiN electrode is 80 nm and the thickness of $Ce_{0.8}Gd_{0.2}O_{1.9}$ within Au/CGO/TiN and TiN/CGO/TiN thin films are 800 and 1400 nm, respectively (Fig. S2 of the supplementary material). The top electrode in the former (Au) and the latter (TiN) is 120 and 50 nm, respectively. The CGO layers exhibit a preferred (111) orientation (Fig. S1 of the supplementary material), as consistent with that prepared by RF sputtering,[10,24] and show a columnar structure with no detectable porosity. The electromechanical characterization with a cantilever vibration setup is shown in Fig. 1(c).

Figure 2 shows the oscillating response of the Au/CGO/TiN and TiN/CGO/TiN under the application of alternating electric fields (25 and 27 kV/cm) at f_E = 100 mHz. The measurements indicate that the films expand perpendicularly to the electric field, developing in-plane stress. As already highlighted in previous works,[9–11,24] the in-plane expansion is a peculiar behavior in CeO_2-based electrostrictive materials, as the characteristic second harmonic oscillation,[21] found at a frequency of $2{\cdot}f_E$ = 200 mHz. Electrostriction in other materials is usually attributed to possible Maxwell-tensor and/or thermal Joule effects.[45] For the Maxwell tensor effect, these are observed in polymers and it is generally negligible in hard inorganic materials,[46] and thus, its contribution to the in-plane stress resulting by the out-of-plane electric field is surely null.[45] On the other hand, the Joule effect due to the thermal expansion-driven bending is difficult to be distinguished and isolated from electromechanical oscillation. Both thermal expansion and electrostriction in CGO develop tensile in-plane stress and quadratic

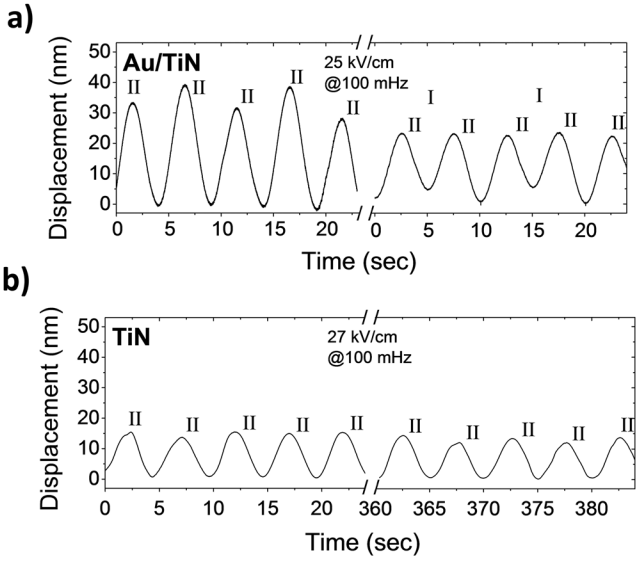

FIG. 2. Cantilever vertical displacement at the free end with 100 mHz applied electric field. II and I indicate the contribution from the second harmonic (200 mHz) and the first harmonic (100 mHz), respectively. (a) Displacements of Au/CGO/TiN at 25 kV/cm at the initial condition (left) and after consecutive measurements (right). (b) Displacements of TiN/CGO/TiN at 27 kV/cm as a function of measuring time.

dependence with respect to the electric field. In our case, however, the thermal contribution to the total displacement is negligible as its calculated value was found to be low (~0.1 nm for Au/CGO/TiN and ~0.5 nm for TiN/CGO/TiN) and no temperature increase was detected with the thermal camera. The contribution of the mechanical resonance can also be excluded due to the higher resonance frequency than that of oscillation (>1 kHz vs 200 mHz).

At the initial stage of the experiments, the electrostriction coefficients of the Au/CGO/TiN and the TiN/CGO/TiN are similar, with the field electrostriction coefficient being $M_e = 2.3 \pm 0.3 \times 10^{-18}$ m^2/V^2 and $M_e = 1.5 \pm 0.2 \times 10^{-18}$ m^2/V^2, respectively. These values are very high and fully consistent with the other values reported for this class of materials.[9–12,24]

In order to evaluate the stability of the performances of the samples, we included the oscillation in the late part of the experiment, after several repeating and measuring times. Figure 2(a) shows that continuous voltage stress causes a decrease in the oscillation of Au/CGO/TiN thin films, which displays a double first and second harmonics oscillation. The double harmonics behavior should rise only in samples subjected to *AC* (E_{ac}) and *DC* (E_{dc}) electric fields simultaneously. Under this condition, the harmonic evolution of stress is proportional to two periodic terms,[9]

$$\sigma \propto \{E_{ac}\cos(\omega t) + E_{dc}\}^2 = E_{dc}^2 + \frac{E_{ac}^2}{2} + 2E_{ac}E_{dc}\cos(\omega t) + \frac{E_{ac}^2}{2}\cos(2\omega t), \quad (5)$$

with $\omega = 2\pi f$ being the angular frequency of applied field. The first harmonic behavior has been ascribed to an internal bias (E_{int}) in the sample, which is generally attributed to the different quality of

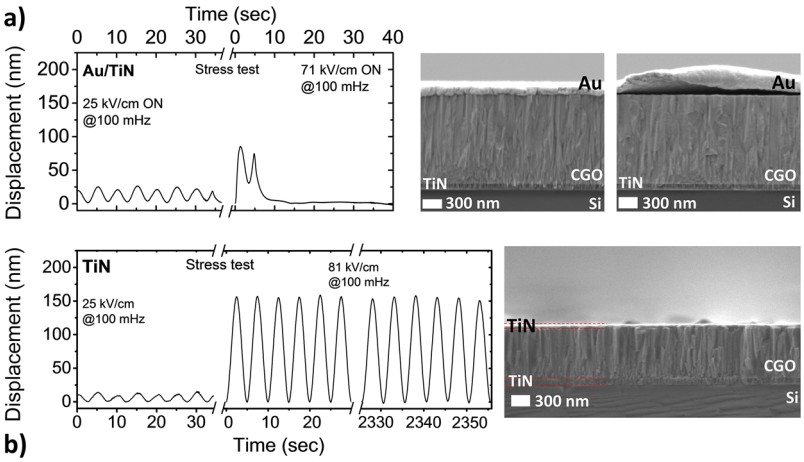

FIG. 3. (a) Stress test on a TiN/CGO/Au thin film: (*left*) beam displacement at 25 kV/cm, displaying the failure at 71 kV/cm; (*middle*) FE-SEM cross section images with the Au top electrode still adherent to the film; (*right*) postmortem cross section showing top electrode detachment caused by voltage stress. (b) Stress test of the TiN/CGO/TiN thin film; (*left*) beam displacement at 25 kV/cm and 81 kV/cm over 40 min showing high stability; (*right*) FE-SEM cross section image after stress test, showing TiN electrodes still perfectly adhered to the CGO film.

the two electrodes.[26] Figure 2(a) also shows that at the early stage of the measurements, only the second harmonic contribution was detected. This suggests a development of internal bias contribution E_{int} caused by continuous electric field stress. A possible reason for the appearance of the internal electric field and decreased oscillation magnitude can thus be ascribed to the possible degradation of the electrode and CGO/electrode interfaces. The decrease in the oscillations yields to a decreased electrostriction coefficient, i.e., $M_e = 1.50 \pm 0.03 \times 10^{-18}$ m^2/V^2, which is still comparable with the early values. On the other hand, TiN/CGO/TiN thin films did not show any sign of degradation over a long period of time, as demonstrated by their displacements as a function of time [Fig. 2(b)]. The oscillation is stable in the amplitude and is only the II harmonic dependent, which excludes the degradation of the electrodes or the development of internal bias, demonstrating the reliability of TiN electrodes as a function of time.

In order to investigate the film stability, under high voltage stress, we applied an alternating electric field of 71 kV/cm and 81 kV/cm (f = 100 mHz for both cases) to Au/CGO/TiN and TiN/CGO/TiN thin films, respectively. Figure 3(a) (*left*) shows that as soon as the higher voltage was applied, the sample displayed a high oscillation over a very short time after which no mechanical response was detected. The resistance of the sample increased to 100–200 MΩ and it did not recover over time, which may indicate mechanical damage in the structure involving the film, the electrodes, or the interfaces. *Postmortem* SEM analysis on the sample [Fig. 3(a) on the right] shows no cracks in the CGO film. This was expected as others reported even higher operating electric fields.[10,24] The TiN bottom electrodes did not show visible degradation while a clear failure was observed at the Au top electrode, which should be responsible for the deterioration of performances. The stability of the TiN electrodes is further confirmed by the outcome of the stress test for the TiN/CGO/TiN sample: Figure 3(b) shows an exceptional stability at a high field, 81 kV/cm. No visible degradation of the displacements was observed over a rather long measuring time (e.g., 40 min). SEM cross section observations confirm that the films and interfaces remained intact, indicating an exceptional good coupling between the CGO and TiN and points out to the direction of integrating the CGO with Si technology using TiN electrodes.

In summary, the effects of ceramic electrodes on the electrostrictive response and stability of CGO films were investigated using a hybrid metal-ceramics configuration, using Au/TiN as electrodes, and a full ceramic device (TiN/TiN). Electromechanical properties were studied using beam deflection technique, and an active response was observed for both Au/CGO/TiN and TiN/CGO/TiN samples, with electrostriction coefficients of $M_e = 2.3 \times 10^{-18}$ m^2 V^{-2} and $M_e = 1.5 \times 10^{-18}$ m^2 V^{-2}, respectively. Our study shows a decrease in the performances and internal stability of the sample with the metal electrode. TiN/CGO/TiN on the other hand displayed good durability. On an electromechanical stress-test, we show a critical failure of Au/CGO/TiN caused by the detachment of the metal electrode at 71 kV/cm. On the other hand, TiN/CGO/TiN was stable up to 81 kV/cm, with no signs of degradation or mechanical failures. Our results indicated excellent mechanical integrity between the TiN electrodes and the CGO film. TiN is found to be a very promising electrode on Si and, therefore, is of particular interest for further investigation as a platform for growing CGO thin films.

See supplementary material for structural characterization by X-ray diffraction and SEM cross section.

This research was supported by the Danish Council for Independent Research Technology and Production Sciences for the DFF-Research Project 2 (Grant No. 48293) and the BioWings project funded by the European Union's Horizon 2020, Future and Emerging Technologies (FET) programme (Grant No. 801267).

REFERENCES

[1] S. H. Baek, J. Park, D. M. Kim, V. A. Aksyuk, and R. R. Das, Science **334**, 958 (2011).
[2] G. H. Haertling, J. Am. Ceram. Soc. **82**, 797 (1999).
[3] A. L. Kholkin, E. K. Akdogan, A. Safari, P. F. Chauvy, and N. Setter, J. Appl. Phys. **89**, 8066 (2001).
[4] N. Ledermann, P. Muralt, J. Baborowski, S. Gentil, K. Mukati, M. Cantoni, A. Seifert, and N. Setter, Sens. Actuators, A **105**, 162 (2003).
[5] R. A. Dorey and R. W. Whatmore, J. Electroceram. **12**, 19 (2004).
[6] A. Schatz, D. Pantel, and T. Hanemann, J. Appl. Phys. **122**, 114502 (2017).
[7] D. Isarakorn, A. Sambri, P. Janphuang, D. Briand, and S. Gariglio, J. Micromech. Microeng. **20**, 055008 (2010).

[8]M. D. Nguyen, H. Yuan, E. P. Houwman, M. Dekkers, G. Koster, J. E. ten Elshof, and G. Rijnders, ACS Appl. Mater. Interfaces **8**, 31120 (2016).
[9]R. Korobko, A. Patlolla, A. Kossoy, E. Wachtel, H. L. Tuller, A. I. Frenkel, and I. Lubomirsky, Adv. Mater. **24**, 5857 (2012).
[10]R. Korobko, E. Wachtel, and I. Lubomirsky, Sens. Actuators, A **201**, 73 (2013).
[11]A. D. Ushakov, N. Yavo, E. Mishuk, I. Lubomirsky, V. Y. Shur, and A. L. Kholkin, KnE Mater. Sci. **1**, 177 (2016).
[12]R. Korobko, A. Lerner, Y. Li, E. Wachtel, A. I. Frenkel, and I. Lubomirsky, Appl. Phys. Lett. **106**, 042904 (2015).
[13]A. Kabir, S. Santucci, N. Van Nong, M. Varenik, I. Lubomirsky, R. Nigon, P. Muralt, and V. Esposito, Acta Mater. **174**, 53 (2019).
[14]C. Sun, H. Li, and L. Chen, Energy Environ. Sci. **5**, 8475 (2012).
[15]A. Kossoy, Q. Wang, R. Korobko, V. Grover, Y. Feldman, E. Wachtel, A. K. Tyagi, A. I. Frenkel, and I. Lubomirsky, Phys. Rev. B **87**, 054101 (2013).
[16]R. E. N. V. Sundar, J.-F. Li, and D. Viehland, Mater. Res. Bull. **31**, 555 (1996).
[17]F. Li, L. Jin, Z. Xu, and S. Zhang, Appl. Phys. Rev. **1**, 011103 (2014).
[18]A. You, M. A. Y. Be, and I. In, **202902**, 0 (2017).
[19]A. Hussain, A. Maqbool, R. A. Malik, M. H. Kim, T. K. Song, and W. J. Kim, IOP Conf. Ser.: Mater. Sci. Eng. **146**, 012006 (2016).
[20]N. Yavo, A. D. Smith, O. Yeheskel, S. Cohen, R. Korobko, E. Wachtel, P. R. Slater, and I. Lubomirsky, Adv. Funct. Mater. **26**, 1138 (2016).
[21]R. E. Newnham, V. Sundar, R. Yimnirun, J. Su, and Q. M. Zhang, J. Phys. Chem. B **101**, 10141 (1997).
[22]E. Wachtel and I. Lubomirsky, Scr. Mater. **65**, 112 (2011).
[23]Y. Li, O. Kraynis, J. Kas, T. C. Weng, D. Sokaras, R. Zacharowicz, I. Lubomirsky, and A. I. Frenkel, AIP Adv. **6**, 055320 (2016).
[24]M. Hadad, H. Ashraf, G. Mohanty, C. Sandu, and P. Muralt, Acta Mater. **118**, 1 (2016).
[25]E. Mishuk, E. Makagon, E. Wachtel, S. R. Cohen, R. Popovitz-Biro, and I. Lubomirsky, Sens. Actuators, A **264**, 333 (2017).
[26]A. D. Ushakov, E. Mishuk, E. Makagon, D. O. Alikin, A. A. Esin, I. S. Baturin, A. Tselev, V. Y. Shur, I. Lubomirsky, and A. L. Kholkin, Appl. Phys. Lett. **110**, 142902 (2017).
[27]A. Bieberle-Hütter, J. L. Hertz, and H. L. Tuller, Acta Mater. **56**, 177 (2008).
[28]N. Pryds, K. Rodrigo, S. Linderoth, and J. Schou, Appl. Surf. Sci. **255**, 5232 (2009).
[29]V. Esposito, D. W. Ni, S. Sanna, F. Gualandris, and N. Pryds, RSC Adv. **7**, 13784 (2017).
[30]J. E. Sundgren, Thin Solid Films **128**, 21 (1985).
[31]N. K. Ponon, D. J. R. Appleby, E. Arac, P. J. King, S. Ganti, K. S. K. Kwa, and A. O. Neill, Thin Solid Films **578**, 31 (2015).
[32]R. H. Dauskardt, M. Lane, Q. Ma, and N. Krishna, Eng. Fract. Mech. **61**, 141 (1998).
[33]M. C. Lemme, J. K. Efavi, T. Mollenhauer, M. Schmidt, H. D. B. Gottlob, T. Wahlbrink, and H. Kurz, Microelectron. Eng. **83**, 1551 (2006).
[34]M. Lukosius, C. Walczyk, M. Fraschke, D. Wolansky, H. Richter, and C. Wenger, Thin Solid Films **518**, 4380 (2010).
[35]C. N. Kirchner, H. Hallmeier, R. Szargan, T. Raschke, and C. Radehaus, Electroanalysis **19**, 1023 (2007).
[36]M. A. Hopcroft, W. D. Nix, and T. W. Kenny, J. Microelectromech. Syst. **19**, 229 (2010).
[37]V. Shelukhin, I. Zon, E. Wachtel, Y. Feldman, and I. Lubomirsky, Solid State Ionics **211**, 12 (2012).
[38]S. Kim and J. Maier, J. Electrochem. Soc. **149**, J73 (2002).
[39]A. Infortuna, A. S. Harvey, and L. J. Gauckler, Adv. Funct. Mater. **18**, 127 (2008).
[40]J. Schou, Appl. Surf. Sci. **255**, 5191 (2009).
[41]S. Sanna, V. Esposito, D. Pergolesi, A. Orsini, A. Tebano, S. Licoccia, G. Balestrino, and E. Traversa, Adv. Funct. Mater. **19**, 1713 (2009).
[42]K. Rodrigo, S. Heiroth, M. Lundberg, N. Bonanos, K. Mohan Kant, N. Pryds, L. Theil Kuhn, V. Esposito, S. Linderoth, J. Schou, and T. Lippert, Appl. Phys. A **101**, 601 (2010).
[43]R. Chowdhury, R. D. Vispute, K. Jagannadham, and J. Narayan, J. Mater. Res. **11**, 1458 (1996).
[44]D. Rasic, R. Sachan, M. F. Chisholm, J. Prater, and J. Narayan, Cryst. Growth Des. **17**, 6634 (2017).
[45]Y. M. Shkel and D. J. Klingenberg, J. Appl. Phys. **80**, 4566 (1996).
[46]L. Liu and P. Sharma, J. Mech. Phys. Solids **112**, 1 (2018).